Further Improvements to the Statistical Hurricane Intensity Prediction Scheme Using Tropical Cyclone Rainfall and Structural Features

UDAI SHIMADA, HIROMI OWADA, MUNEHIKO YAMAGUCHI, TAKESHI IRIGUCHI, MASAHIRO SAWADA, AND KAZUMASA AONASHI

Meteorological Research Institute, Tsukuba, Ibaraki, Japan

MARK DEMARIA

NOAA/National Hurricane Center, Miami, Florida

KATE D. MUSGRAVE

Cooperative Institute for Research in the Atmosphere, Colorado State University, Fort Collins, Colorado

ABSTRACT

The Statistical Hurricane Intensity Prediction Scheme (SHIPS) is a multiple regression model for forecasting tropical cyclone (TC) intensity [both central pressure (Pmin) and maximum wind speed (Vmax)]. To further improve the accuracy of the Japan Meteorological Agency version of SHIPS, five new predictors associated with TC rainfall and structural features were incorporated into the scheme. Four of the five predictors were primarily derived from the hourly Global Satellite Mapping of Precipitation (GSMaP) reanalysis product, which is a microwave satellite-derived rainfall dataset. The predictors include the axisymmetry of rainfall distribution around a TC multiplied by ocean heat content (OHC), rainfall areal coverage, the radius of maximum azimuthal mean rainfall, and total volumetric rain multiplied by OHC. The fifth predictor is the Rossby number. Among these predictors, the axisymmetry multiplied by OHC had the greatest impact on intensity change, particularly, at forecast times up to 42 h. The forecast results up to 5 days showed that the mean absolute error (MAE) of the Pmin forecast in SHIPS with the new predictors was improved by over 6% in the first half of the forecast period. The MAE of the Vmax forecast was also improved by nearly 4%. Regarding the Pmin forecast, the improvement was greatest (up to 13%) for steady-state TCs, including those initialized as tropical depressions, with slight improvement (2%–5%) for intensifying TCs. Finally, a real-time forecast experiment utilizing the hourly near-real-time GSMaP product demonstrated the improvement of the SHIPS forecasts, confirming feasibility for operational use.

1. Introduction

While the skill of tropical cyclone (TC) intensity forecasts has improved over the past two decades (DeMaria et al. 2014), the improvement rate is lower than that of TC track forecasts (Yamaguchi et al. 2017). There are several reasons for this lower rate of improvement: dynamical and thermodynamical processes and air–sea interactions that govern the intensity change of TCs are very complicated and not completely understood, observations within the inner core of a TC are not necessarily available to forecasters in real time, current numerical models do not necessarily reproduce observed TC structures and intensity changes, and there are uncertainties in TC intensity estimation.

In such challenging situations, the advent of skillful statistical dynamical models has greatly contributed to the improvement of intensity forecasts. The Statistical Hurricane Intensity Prediction Scheme (SHIPS; DeMaria and Kaplan 1994, 1999; DeMaria et al. 2005) is one of the statistical–dynamical models used for intensity forecasts. Since its first implementation for the Atlantic basin in the early 1990s, the skill of SHIPS forecasts has steadily improved. SHIPS is widely used in operational centers around the world and is one of the most

---

ꝺ Denotes content that is immediately available upon publication as open access.

Corresponding author: Udai Shimada, ushimada@mri-jma.go.jp

accurate guidance models for TC intensity forecasts (e.g., Rappaport et al. 2012; Sampson and Knaff 2014).

SHIPS is a multiple regression model that predicts changes in TC intensity. Explanatory variables (hereafter predictors) used in the regression model include climatology and persistence associated with the TC's initial intensity and intensity change in the past 12 h; environmental conditions such as vertical wind shear and sea surface temperatures (SSTs), which are computed along the forecast TC track; and infrared (IR) satellite information around the TC at the initial forecast time. The SHIPS model also provides information about the degree to which each predictor contributes to intensity change in a way that can be examined by forecasters.

In the western North Pacific (WNP) basin, the Statistical Typhoon Intensity Prediction Scheme (STIPS; Knaff et al. 2005), which is similar to SHIPS, was developed and is used at the Joint Typhoon Warning Center (JTWC). Recently, it was replaced with SHIPS at JTWC to take advantage of the higher temporal resolution output and new predictors in SHIPS (Schumacher et al. 2013). More recently, the Meteorological Research Institute (MRI) of the Japan Meteorological Agency (JMA) set up a version of SHIPS that predicts the minimum central pressure (Pmin) as well as the maximum wind speed (Vmax) of TCs in the WNP basin using output from the JMA Global Spectral Model (GSM; see JMA 2018) (Yamaguchi et al. 2018). The forecast results confirmed that the accuracy of SHIPS with the GSM output was 23%–30% better than that of the Statistical Hurricane Intensity Forecast model (SHIFOR; Jarvinen and Neumann 1979; Knaff et al. 2003), which is a statistical model based on climatology and persistence that is often used as a benchmark for the evaluation of intensity forecast skill (e.g., Rappaport et al. 2012; Sampson and Knaff 2014). As of 2017, SHIPS is in experimental use at the Regional Specialized Meteorological Center (RSMC) Tokyo, Japan.

Most of the SHIPS predictors measure the storm environment, based on the idea that intensity change and maximum potential intensity (MPI) primarily depend on environmental conditions. This type of information was also readily available when SHIPS was first developed. Intensity change, however, is also highly dependent on convective activity and the TC's diabatic heating distribution. Observational studies have shown that brightness temperatures T_b and rainfall amounts observed by microwave satellites have a relationship with the current and future intensity (e.g., Rao and MacArthur 1994; Rao and McCoy 1997; Cecil and Zipser 1999; Bankert and Tag 2002; Hoshino and

Nakazawa 2007; Kieper and Jiang 2012). The 85-GHz T_b provides information about the inner-core structure and convective activity, and 19- and 37-GHz T_b provide rainfall information. Cecil and Zipser (1999) showed that the azimuthal mean 85-GHz T_b is related to the future intensity. Hoshino and Nakazawa (2007) found that 10- and 19-GHz T_b distributions were better correlated with TC intensity than 37- and 85-GHz T_b distributions. Kieper and Jiang (2012) used satellite observations to show that the formation of an eyewall ring consisting of low-level water clouds and warm rain is related to subsequent rapid intensification (RI). More recently, Shimada et al. (2017) showed that future intensity change increases with increasing axisymmetry of the inner-core rainfall distribution, using a microwave satellite-based rainfall product, the Global Satellite Mapping of Precipitation (GSMaP; Kubota et al. 2007, 2009).

The importance of the inner-core structure associated with internal processes to TC intensity change has also been verified from other perspectives. Hendricks et al. (2010) showed that there is little difference in the environmental conditions between TCs that experienced RI and those that intensified at a normal rate, and concluded that the intensification rate is controlled mostly by internal dynamical processes, provided that environmental conditions are favorable for intensification. Miyamoto and Takemi (2013) performed an idealized numerical simulation and demonstrated that the axisymmetrization of potential vorticity around a TC is important for the onset of RI. Miyamoto and Takemi (2015) also demonstrated that the time taken for RI onset depends on the Rossby number R_o of vortices at the initial time, and that intensification starts earlier with larger initial R_o. Chen et al. (2011) and Carrasco et al. (2014) showed that the radius of maximum wind (RMW) and the radius of 34-kt winds (1 kt $\approx$ 0.514 m s^{-1}) have a negative correlation with intensity changes in the next 24 h.

Based on these studies, the addition of predictors associated with TC structure has the potential to improve SHIPS, in particular for the following two types of TCs: 1) large-sized, unorganized TCs and 2) intensifying TCs. The former TCs typically originate from monsoon gyres (Lander 1994) or monsoon troughs (Lander 1996). They are characterized as large-scale vortices relative to their maximum wind speed, with a lack of organized convection near the center, and small rates of intensification even in a favorable environment. Since the current version of SHIPS does not explicitly include structural information, when environmental conditions are favorable, it predicts intensification even for monsoon-gyre-type TCs, which can lead to an overforecast of TC

intensity. As for intensifying TCs, the current version of SHIPS tends to underforecast their intensity (e.g., Jones et al. 2006; Sampson and Knaff 2014; Cangialosi and Franklin 2017). Predictors associated with the inner-core structure may increase the rate of intensity change, leading to a better forecast of intensification.

Previous studies have shown that the addition of microwave T_b predictors (e.g., mean T_b and maximum T_b within 100-km radius from the TC center) derived from 19- and 85-GHz T_b data to SHIPS (referred to as SHIPS-MI) can improve its accuracy (Jones et al. 2006, 2007; Jones and Cecil 2007). Jones et al. (2006) showed that a 2%–8% improvement was obtained from SHIPS-MI compared with SHIPS without those predictors. However, issues of temporally sparse microwave satellite observations and their latency prevented the operational implementation of SHIPS-MI. In this study, we resolved these issues by using hourly GSMaP products, one of which is available to operational centers in near–real time at constant time intervals and has a large developmental sample (more than 10 yr) to calculate regression coefficients. We derived new predictors associated with TC rainfall and structure mainly from the GSMaP data.

The purpose of this study is to examine the degree to which the intensity forecast accuracy can be improved if rainfall and structural information are added to SHIPS. In other words, the purpose is to examine how much the rainfall and structural information at the initial time is statistically related to the subsequent intensity change within the framework of a multiple regression model. For this purpose, we mainly used a GSMaP reanalysis product, which has the highest accuracy among the GSMaP family products. Then, we used a near-real-time GSMaP product to examine the feasibility for operational use.

This paper consists of four subsequent sections. We describe the data used and the methods in section 2. In section 3, we present forecast performance results. Section 4 discusses the impact of inner-core structural information on TC intensity forecasts. Section 5 contains a summary.

2. Data and methodology

In this section, we describe data sources of training samples from 2000 to 2012 used for computing coefficients of the regression model, independent samples from 2013 to 2016 used for forecast experiments, and the verification of forecasts. Then, we introduce new predictors associated with the rainfall distribution and structural features, followed by the design of forecast experiments and their verification.
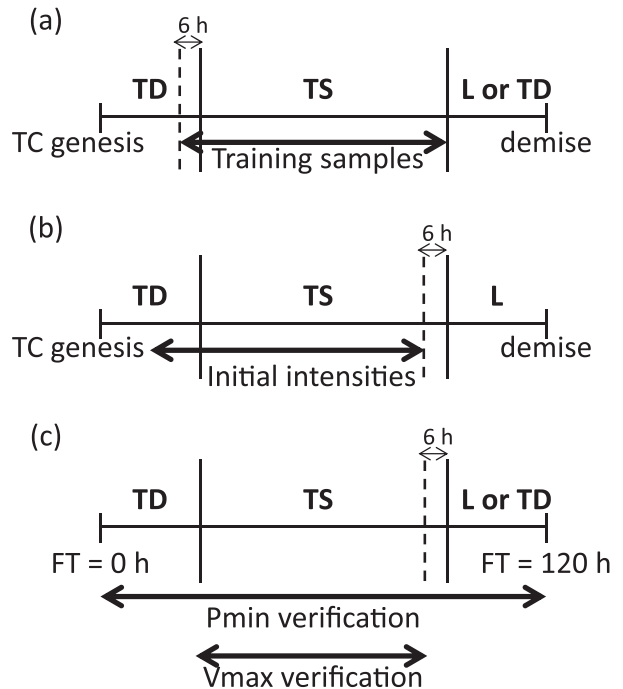

FIG. 1. (a) An example of a TC used for training samples. The abscissa axis represents a storm life cycle from TD strength, through TS strength and above, until extratropical cyclone (L) stage or TD strength. (b) Initial intensities when a forecast is performed. The abscissa axis represents the initial intensities in a storm life cycle from TD strength, through TS strength and above, until the L stage. A forecast is performed as long as the GSM model has a TC at TD strength and above as of FT = 0 h (including a TD that weakened from a TS). (c) The Pmin and Vmax forecasts used for verification. The abscissa axis represents forecast times up to 5 days when storm intensity at FT = 0 h is TD strength.

a. Data

For training samples and other purposes in this study, best track data at 6-h intervals from the RSMC Tokyo were used, including the intensity (both Pmin and Vmax), the center position, and 30-kt wind radii R_{30} (largest and smallest R_{30} in eight orientations) of TCs that attained tropical storm (TS) strength and above during their lifetimes. Wind speeds in the best track data are based on 10-min sustained wind speeds. The best track data do not provide Vmax information for tropical depressions (TDs) (Vmax < 34 kt) and extratropical cyclones. Thus, the training samples included TCs at TS strength and above (Vmax ≥ 34 kt), TDs 6 h before they intensified into TSs, and storms just when they weakened to TDs or extratropical cyclones (Fig. 1a). In the latter two cases, Vmax was assumed to be 30 kt.

Training samples of atmospheric environmental predictors were derived from the Japanese 55-year Reanalysis (JRA-55) data (Kobayashi et al. 2015).

Predictors of IR T_b were derived from successive geostationary satellite data that have been used in the JMA. The SST dataset used to calculate an empirical MPI (DeMaria and Kaplan 1994) was the Centennial Observation-Based Estimates of SST (COBE-SST; Ishii et al. 2005) because it was used for JRA-55 data as the ocean boundary condition. Ocean heat content (OHC) was calculated using ocean data [the Meteorological Research Institute multivariate ocean variational estimation system (MOVE/MRI.COM); Usui et al. (2006)].

We used GSMaP data to extract rainfall and structural information. The data are composed of microwave satellite-based rainfall rate (mm h^{-1}) estimates with a horizontal resolution of 0.1° (Aonashi and Liu 2000; Aonashi et al. 2009; Shige et al. 2009). Microwave satellite data used in GSMaP include the Tropical Rainfall Measuring Mission (TRMM) Microwave Imager (TMI), the *Advanced Earth Observing Satellite-II* (*ADEOS-II*) Advanced Microwave Scanning Radiometer (AMSR), the *Aqua* AMSR for Earth Observing System (AMSR-E), the *Global Change Observation Mission–Water* (*GCOM-W1*) AMSR2, the Global Precipitation Measurement *Core Observatory* (GPM *Core*) Microwave Imager (GMI), the Defense Meteorological Satellite Program (DMSP) Special Sensor Microwave Imager/Sounder (SSM/IS) series, the National Oceanic and Atmospheric Administration (NOAA) Advanced Microwave Sounding Unit series (AMSU), and the Meteorological Operational Satellite Program of Europe (MetOp) AMSU series. The product covers the area from 60°S to 60°N, is available since 2000, and has a range of reanalysis versions, a near-real-time version (about 4-h latency) and a real-time version (almost no latency; JAXA 2018a). These data are processed and provided by the JAXA (JAXA 2018b). Because the temporal resolution of microwave satellite-derived rainfall estimates at each point is about 3–6 h, hourly estimates are obtained by two temporal interpolation methods: the morph method and rainfall correction by use of a Kalman filter (Ushio et al. 2009). Details of GSMaP data for TC research are described by Shimada et al. (2017). For training samples, we used the hourly reanalysis product (the version 6 algorithm without the gauge correction).

For independent samples in forecast experiments (also see section 2c), we utilized data that had been available to RSMC Tokyo in real time. Real-time TC data at 6-h intervals generated by RSMC Tokyo were used, including the intensity, the center position, and R_{30}. JMA GSM forecasts were used for atmospheric environmental predictors. The domain of the data archived was from 10°S to 65°N and from 80°E to 170°W at a spatial resolution of 0.2° latitude and 0.25° longitude.

TABLE 1. SHIPS predictors used in SHIPS-Base. Predictors retained in the Pmin and Vmax models are denoted with a P or V, respectively.

Predictor	Description	Model
1) MSLP	Pmin at FT = 0 h	P, V
2) VMAX	Vmax at FT = 0 h	—
3) VMA2	Square of VMAX	V
4) OSLP	Absolute of (MSLP − 970)	P
5) PER	12-h change in Pmin or Vmax	P, V
6) PMPE	(MSLP − 880) × PER	P
7) VMPE	VMAX × PER	V
8) POT	MPI − VMAX	P, V
9) POT2	Square of POT	P, V
10) COHC	Ocean heat content	P, V
11) OHC2	Square of COHC	P, V
12) T200	200-hPa temperature (r = 200–800 km)	P, V
13) T250	250-hPa temperature (r = 200–800 km)	P, V
14) ZNAL	Zonal storm motion	P, V
15) RHMD	700–500-hPa relative humidity (%) (r = 200–800 km)	P, V
16) EPOS	θ_e difference between lifted surface parcel and environment	P, V
17) SHDC	850–200-hPa vertical shear magnitude (r = 0–500 km)	P, V
18) SHGC	Generalized vertical shear parameter (DeMaria 2010)	P, V
19) SHSH	Square of SHDC	P, V
20) SHLT	SHDC × the sine of latitude	P, V
21) SHVM	SHDC/VMAX	P, V
22) VMSH	VMAX × SHDC	V
23) PMSH	(MSLP − 880) × SHDC	P
24) Z850	850-hPa absolute vorticity (r = 0–1000 km)	P, V
25) D200	200-hPa divergence (r = 0–1000 km)	P, V
26) TWAT	Tendency of 850-hPa tangential wind (r = 0–500 km)	P, V
27) TADV	Temperature advection between 850 and 700 hPa (r = 0–500 km)	P, V
28) TGRD	Magnitude of temperature gradient between 850 and 700 hPa (r = 0–500 km)	P, V
29) PC30	Percent area of IR T_b < −30°C (r = 50–200 km)	P, V
30) SDIR	Standard deviation of IR T_b (r = 0–200 km)	P, V

The GSM ran four times a day at 0000, 0600, 1200, and 1800 UTC. The GSM initialized at 1200 UTC ran to 11 days, and the others ran to 84 h from 2013 to 2015 and to 132 h in 2016.[1] Thus, the number of forecast samples decreased beginning from the 90-h forecast time (FT) (FT = 90 h) through 5 days (FT = 120 h). The Merged Satellite and In Situ Data Global Daily Sea Surface Temperature dataset (MGDSST; Kurihara et al. 2006)

---

[1] The 132-h model run was experimental and not for operational use in 2016.

TABLE 2. Added predictors to SHIPS-GSMaP and excluded predictors. Predictors retained in the Pmin and Vmax models are denoted with a P or V, respectively.

In/out	Predictor	Description	Model
In	31) AXIS	Axisymmetry of rainfall structure within 300-km radius × OHC	P, V
In	32) RCOV	Rain percent area coverage between 100- and 300-km radius	P
In	33) RCOV	Rain percent area coverage within 300-km radius	V
In	34) RMAX	Radius of maximum azimuthal mean rainfall	P, V
In	35) RVOL	Total volumetric rain within 100-km radius × OHC	P
In	36) RVOL	Total volumetric rain between 100- and 300-km radius × OHC	V
In	37) ROSB	Rossby number	P, V
Out	29) PC30	Percent area of IR $T_b < -30°C$ ($r = 50$–200 km)	—
Out	30) SDIR	Standard deviation of IR T_b ($r = 0$–200 km)	—

was used for the empirical MPI because it was the GSM ocean boundary condition. OHC was calculated using the same data as the training data. As for the GSMaP data, both the GSMaP reanalysis product and near-real-time product (~4-h latency) were used. Rainfall estimates of the reanalysis product are based on both past and future satellite data, while estimates of the near-real-time product are based only on past data. Thus, data quality is much better for the former than for the latter. We show the impact of GSMaP data used for the intensity forecasts in section 3c.

b. New predictors

Most predictors used in the current version of SHIPS with the GSM output (hereafter SHIPS-Base) are the same as those of SHIPS used in the United States (Table 1). Table 2 lists five new predictors that were added to the Vmax and Pmin versions of SHIPS-Base (hereafter SHIPS-GSMaP). The IR T_b-related predictors were removed because the accuracy was reduced when they were included with the GSMaP predictors. Among the five new predictors, four were mainly derived from GSMaP data: axisymmetry of rainfall, rainfall areal coverage, radius of maximum rainfall, and total volumetric rain. The value of R_o was derived from TC data provided by the RSMC Tokyo.

These five predictors were selected by performing stepwise regression (forward, backward, and stepwise selections) using International Mathematics and Statistics Library (IMSL) software. Initially, we prepared the 26 conventional predictors listed in Table 1 and 15 possible new predictors associated with rainfall amount

and structural features. These predictors were fed into the regression. We counted the number of times each predictor was retained during the forecast period up to 120 h at 6-h intervals in the three kinds of stepwise regressions. Then, predictors that had relatively high frequencies (at least more than 20%[2]) of selection in the stepwise regressions were determined as new predictors. The selected new predictors are defined below.

The axisymmetry γ is the same as that of Miyamoto and Takemi (2013) and is defined as

$$\gamma(r,t) \equiv \frac{\overline{\phi}^{\lambda}(r,t)^2}{\overline{\phi}^{\lambda}(r,t)^2 + \int_0^{2\pi} \phi'(r,\lambda,t)^2\, d\lambda/2\pi} \times 100, \quad (1)$$

where ϕ is a variable; r and λ are the radial and tangential directions, respectively; and t is time. We used the rainfall rate from the GSMaP dataset for ϕ in this study. The azimuthal mean (axisymmetric component) of ϕ is denoted by an overbar, and the deviation from the azimuthal mean is denoted by a prime. We tested three types of axisymmetry variables: an average over 0–300-km radius from the center, an average over 0–100-km radius, and an average over 100–300-km radius. Among the three axisymmetry predictors, we found that the first one had the highest frequency of selection in the stepwise regression.

Rainfall areal coverage is defined as the percent area of rainfall over $0.1\,\mathrm{mm\,h^{-1}}$ in a specific region. As with axisymmetry, three regions were prepared: a region over 0–300-km radius from the center, a region over 0–100-km radius, and a region over 100–300-km radius. For the Pmin forecast, a radius of 100–300 km from the center, whose region is usually outside of the RMW, was selected in the stepwise regression. For the Vmax forecast, a radius of 0–300 km from the center was selected. This parameter expresses the density of the rainfall area.

The radius of maximum rainfall is defined as the radius of the azimuthal mean maximum rainfall within 400-km radius from the center. This parameter is extracted as a proxy for the RMW.

Total volumetric rain is the sum of rainfall in a specific region. The same three regions as the rainfall areal coverage were prepared. For the Pmin forecast, a radius of 0–100 km from the center was selected in the stepwise regression. For the Vmax forecast, a radius of 100–300 km from the center was selected. This parameter is a proxy for the magnitude of diabatic heating.

---

[2] This value was set so that the one that had the highest frequency of selection among three similar types of variables could be determined.

The amplitudes of a wavenumber-1 rainfall asymmetry averaged over each of the three regions described above were also examined. However, none of the three parameters were retained with relatively high frequency (more than 20%) of selection in the stepwise regression.

The parameters derived from the GSMaP data were obtained at 1-h intervals, but we applied a 5-h running mean (FT = −5 ~ 0 h) to eliminate biases dependent on the satellite data used in the hourly GSMaP data. Shimada et al. (2017) showed that biases between satellites can be eliminated if a 6-h running mean is applied and that the effective signal related to intensity change can be detected by the running mean.

Generally, R_o is defined as

$$R_o \equiv \frac{\text{Vmax}}{R_m f}, \qquad (2)$$

where R_m is the RMW, and f is the Coriolis parameter. Unfortunately, the best track data used in this study do not have RMW information. Instead of R_m, we prepared two alternatives: the use of R_{30} and the use of $15 \times R_{30}/\text{Vmax}$, which is equivalent to R_m derived from R_{30} and the Rankine vortex structure. The stepwise regression selected the use of R_{30}. For TDs, we used a value of 176 km as R_{30}, the mean value of the smallest R_{30} of TCs with a Vmax of 35 kt in the training sample.

The new parameters have values at FT = 0 h and are not dependent on forecast times. However, no matter how favorable the rainfall and structural conditions are at the initial time for subsequent intensification, a TC does not intensify unless favorable environmental conditions are maintained along the future track. In fact, we found that when each value of the axisymmetry and total volumetric rainfall was multiplied by OHC along a forecast track, the accuracy improved. In addition, the multiplication of the total volumetric rainfall by OHC can avoid multicollinearity between the total volumetric rain and the rainfall areal coverage.[3] Thus, we decided to multiply each value of those two parameters by OHC (Table 2). In section 3a, we will present this effect on the improvement of accuracy.

Training samples for the period from 2000 to 2012 were used to calculate coefficients for SHIPS-Base and SHIPS-GSMaP. The predictors were normalized by subtracting their means and dividing by their standard deviations. This normalization enables us to compare the magnitude of coefficients for different predictors. Figure 2 shows the relative contributions of the new

predictors to intensity change. The magnitude of the axisymmetry (AXIS) coefficients in the first half of the forecast period is generally greatest among the new predictors and is one of the 5–10 strongest predictors out of 29 predictors.

The AXIS of Pmin contributes to intensification from FT = 6 to 84 h when its value is above average, whereas it contributes to weakening after FT = 90 h when its value is above average (Fig. 2a). Other new predictors of Pmin contribute slightly to intensity change. Rain percent area coverage (RCOV), total volumetric rain (RVOL), and Rossby number (ROSB) contribute to intensification when each value is above average. The radius of maximum rainfall (RMAX) contributes to intensification from FT = 6 to 66 h and contributes to weakening after FT = 72 h when its value is below average (i.e., smaller radius of maximum rainfall), although the magnitudes of the RMAX coefficients are quite small.

Contributions of RMAX and RVOL to Vmax change differ from those of Pmin change (Fig. 2b). The RMAX of Vmax contributes to intensification throughout the forecast period when its value is below average (i.e., smaller radius of maximum rainfall). RVOL contributes to weakening from FT = 6 to 48 h and contributes to intensification after FT = 54 h when its value is above average.

The signs of the coefficients of the new predictors are generally physically reasonable and consistent with previous studies. AXIS is consistent with the results of Miyamoto and Takemi (2013), Zagrodnik and Jiang (2014), Alvey et al. (2015), and Shimada et al. (2017), who showed that symmetric structure is correlated with intensification. RCOV and RVOL of Pmin are consistent with the results of Jiang and Ramirez (2013), who found that rainfall in the inner-core region is at least moderate to heavy (i.e., total raining area > 3000 km², total volumetric water > 5000 mm h⁻¹ km²) in TCs before the onset of RI. RMAX is consistent with the findings of Chen et al. (2011) and Carrasco et al. (2014), under the assumption that RMAX is a proxy for the RMW. ROSB is consistent with the findings of Miyamoto and Takemi (2015).

c. Design of the forecast experiments and their verification

Forecast experiments were performed for TCs over the ocean from 2013 to 2016, completely independent of the training samples. Two kinds of SHIPS-GSMaP forecasts were run. One used the reanalysis GSMaP product to examine how much the accuracy improves when the quality of rainfall and structural information is as good as possible. Center positions used to extract

---

[3] The correlation coefficient between the total volumetric rain and the rainfall areal coverage was ~0.3.
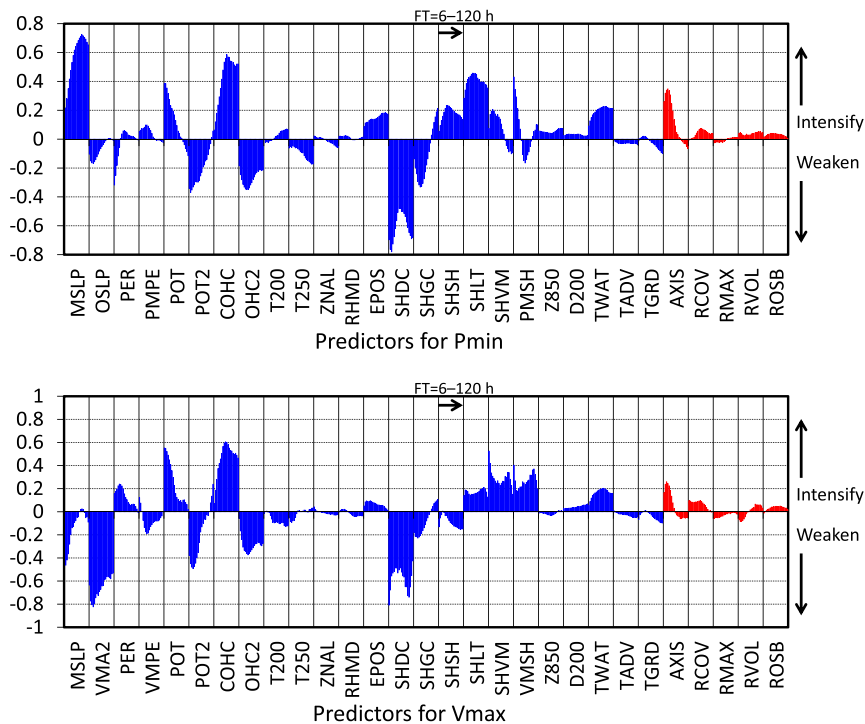
FIG. 2. (a) Normalized SHIPS-GSMaP predictor coefficients for Pmin from FT = 6 to 120 h. All predictor coefficients of FT = 6–120 h are plotted in each predictor box. The sign of each coefficient is reversed so that a positive coefficient contributes to the decrease in Pmin (i.e., intensification) when the corresponding predictor value is above average. (b) As in (a), but for Vmax. A positive coefficient contributes to the increase in Vmax when the corresponding predictor value is above average. The new predictors are indicated by the red color.

parameters from GSMaP data were taken from the best track data. Similarly, the Rossby number was computed by using the best track data. The other used the near-real-time product to examine the feasibility of SHIPS-GSMaP for operational use (hereafter "real-time SHIPS-GSMaP" to discriminate between two SHIPS-GSMaP forecasts). In real-time SHIPS-GSMaP, the center positions were from the real-time TC data. The Rossby number was also computed by using the real-time TC data. The latencies of the near-real-time GSMaP product and the GSM output are almost the same (~4 h), which makes it possible to run real-time SHIPS-GSMaP operationally.

Forecasts were made for TCs that were recorded in the best track data (Fig. 1b). The forecasts included systems that were at least TDs as of FT = 0 h. A forecast was continued up to 5 days as long as the GSM predicted the existence of the system (even if it evolved into an extratropical cyclone in the model) and the system was within the domain of the archived GSM data. However, the forecast was stopped after a TC made landfall in the GSM forecast or when environmental predictors were not computed due to the limitations of the data domain,

including predictors calculated out to a radius of 1000 km from the center of the TC. For practical use of SHIPS, when Pmin was forecast to be above 1010 hPa, the Pmin forecast was corrected to 1010 hPa. Similarly, when Vmax was forecast to be below 30 kt, Vmax was corrected to 30 kt. This correction is justified because the GSM still forecasts the existence of the storm at that time. We confirmed that the impact of this correction on the rate of improvement in SHIPS was negligible (not shown).

For verification, SHIPS forecasts were compared to the best track data. If there was no reference data in the best track, the forecasts were excluded from the verification. For Pmin forecasts, the verification included all TCs and extratropical cyclones that were recorded in the best track data (Fig. 1c), provided that SHIPS forecast them. The timing of the extratropical transition is, in general, different between the real-time and best track data. We considered that to evaluate the effect of the new predictors during the weakening stage including extratropical transition, it is convenient for verification to include storms that had already experienced extratropical transition in the best track data. For Vmax

TABLE 3. Actual sample sizes N, effective sample sizes N_e, lag-1 autocorrelation coefficients ρ_1, averages of the difference in absolute errors between SHIPS-Base and SHIPS-GSMaP, and Student's t statistic t for Pmin and Vmax, respectively. Boldface values in the t-statistic column are statistically significant at the 95% significant level with a two-sided test.

	Pmin					Vmax				
FT (h)	N	N_e	ρ_1	Diff in MAE	t	N	N_e	ρ_1	Diff in MAE	t
6	2438	774	0.52	0.09	**3.49**	2012	759	0.45	0.03	1.16
12	2362	636	0.58	0.23	**4.92**	1978	621	0.52	0.12	**2.75**
18	2273	564	0.60	0.39	**5.51**	1930	526	0.57	0.22	**3.32**
24	2172	420	0.68	0.57	**5.29**	1859	390	0.65	0.33	**3.44**
30	2073	321	0.73	0.67	**4.55**	1766	310	0.70	0.36	**2.95**
36	1982	251	0.78	0.73	**3.86**	1673	242	0.75	0.37	**2.52**
42	1881	198	0.81	0.74	**3.38**	1579	213	0.76	0.37	**2.36**
48	1798	180	0.82	0.70	**3.06**	1493	184	0.78	0.39	**2.44**
54	1711	165	0.82	0.63	**2.82**	1399	166	0.79	0.36	**2.23**
60	1628	147	0.83	0.57	**2.57**	1325	143	0.81	0.36	**2.14**
66	1547	127	0.85	0.58	**2.54**	1247	128	0.81	0.33	**2.00**
72	1470	120	0.85	0.53	**2.40**	1166	112	0.82	0.30	1.79
78	1398	110	0.85	0.45	**2.12**	1092	98	0.84	0.32	1.80
84	1316	100	0.86	0.34	1.52	1020	98	0.82	0.32	1.61
90	471	91	0.68	0.45	**1.99**	367	87	0.62	0.38	1.94
96	433	87	0.66	0.41	1.72	340	81	0.61	0.30	1.54
102	406	76	0.68	0.41	1.64	316	74	0.62	0.30	1.45
108	377	86	0.63	0.45	1.94	284	77	0.58	0.23	1.12
114	349	89	0.59	0.42	1.89	260	70	0.58	0.20	0.99
120	323	63	0.67	0.39	1.61	237	55	0.62	0.19	0.97

forecasts, the verification included all forecasts that had reference Vmax data in the best track. In a case where a storm was of TD strength as of FT = 0 h but it intensified to TS strength at a certain forecast time, forecasts after that time were included in the verification (Fig. 1c).

We applied paired Student's t-test statistics with a two-sided test to confirm the improvement of the accuracy, given a null hypothesis that the average of the difference in absolute errors between SHIPS-Base and SHIPS-GSMaP is zero. Here, we have to consider the number of samples. As pointed out by Aberson and DeMaria (1994), we cannot assume that all forecasts are completely independent because forecasts for the same TC can be correlated. For example, a forecast error at FT = 48 h initialized at a particular time can be correlated to that at FT = 48 h initialized at 6 h later for the same TC. In this study, following a method developed by Wilks (2006) and Jones et al. (2006), we calculated lag-1 (i.e., 6-h lag) autoregression to forecast errors at a particular forecast time and we introduced the effective sample size N_e as

$$N_e = N \frac{(1 - \rho_1)}{(1 + \rho_1)}, \quad (3)$$

where N is the actual sample size and ρ_1 is the lag-1 autoregression coefficient. Table 3 lists results of ρ_1 and N_e. The correlation coefficients lay between 0.4 and 0.9,

which led to the large decrease in the number of samples. Nevertheless, the number of samples was greater than 80 up to FT = 96 h, which was sufficient to perform a significance test.

Intensity change based on the best track data was used to classify TCs as steady state, intensifying, and weakening, following the definitions used in Jones et al. (2006); TCs with Pmin changes < -10 hPa (or Vmax changes ≥ 15 kt) over a particular forecast duration (from the initial time to each forecast time) are classified as intensifying TCs, TCs with Pmin changes $> +10$ hPa (or Vmax changes ≤ -15 kt) are weakening TCs, and others are steady-state TCs. Note that by definition, there are cases that are classified as steady-state TCs that actually experience both intensification and weakening during the forecast period. However, because SHIPS is a model for predicting intensity change over a particular period, this definition is reasonable for verifying the performance of SHIPS.

3. Forecast results

In this section, we show the model performance. We mainly show the results of Pmin forecasts for which the addition of the new predictors had a larger impact on the improvement than for the Vmax forecasts. First, we show the results when the GSMaP reanalysis product was used. Then, we present some forecast examples and
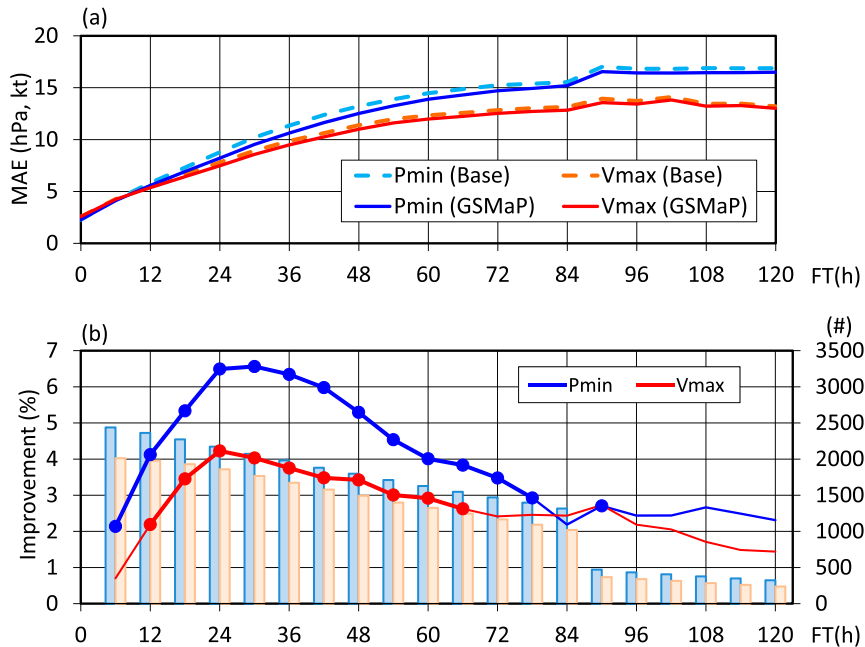
FIG. 3. (a) MAEs (hPa for Pmin, kt for Vmax) of SHIPS-Base and SHIPS-GSMaP forecasts up to 5 days ahead for independent samples from 2013 to 2016 for the WNP basin. (b) Percent improvement of SHIPS-GSMaP MAEs relative to SHIPS-Base MAEs from 2013 to 2016 in the WNP basin (blue and red lines). Bold lines with filled circles indicate statistically significant differences at the 95% level. The bar chart shows the number of samples (light blue for Pmin, light orange for Vmax).

discuss what is improved and what is unresolved. Finally, we show the results of real-time forecasts.

a. Forecast performance

We compared SHIPS-GSMaP with SHIPS-Base (Table 3; Fig. 3). The performance of Pmin and Vmax at each forecast time in SHIPS-GSMaP (Fig. 3a) showed that the mean absolute error (MAE) of Pmin was 12.5 hPa at FT = 48 h, 14.7 hPa at FT = 72 h, and ~16.5 hPa after FT = 90 h. The MAE of Vmax was 11.0 kt at FT = 48 h and ~13 kt after FT = 72 h. The discontinuity of the MAE between FT = 84 and 90 h is due to the decrease in the number of GSM forecasts during the years 2013–15, as described in section 2a. The MAEs of Pmin and Vmax in SHIPS-GSMaP were smaller than those in SHIPS-Base for all forecast times. The improvement rate (Fig. 3b) indicated that the Pmin forecasts in SHIPS-GSMaP outperformed those of SHIPS-Base by 2%–7%, while the Vmax forecasts improved by 1%–4%. The improvement was statistically significant at the 95% confidence level for Pmin forecasts for the period FT = 6–78 h and for Vmax for the period FT = 12–66 h. The improvement in Pmin was greater than that of Vmax up to FT = 78 h. Improvement was maximized at FT = 30 h for Pmin (just over

6%) and at FT = 24 h for Vmax (near 4%). Thus, rainfall and structural information at FT = 0 h definitely improved the accuracy of SHIPS, mainly in the first half of the forecast period. This result is consistent with that of Jones et al. (2006).

We examined the reason why the improvement rates for Pmin and Vmax were different. The verification of Pmin forecasts in Fig. 3b included TD cases at FT = 0 h (Fig. 1c). If the verification was performed only for TD cases at FT = 0 h, the improvement rate became very high, reaching ~20% (Fig. 4a). For non-TD cases at FT = 0 h, the improvement rates of Pmin and Vmax were almost the same (Fig. 4b). The great improvement for TD cases was caused by the suppression of overforecasting (i.e., negative biases) of Pmin for steadystate and intensifying TCs (Fig. 5a). In contrast, for non-TD cases (Fig. 5b), intensifying TCs had positive biases (i.e., underforecasting) for Pmin, which were not decreased by the new predictors. In addition, for nonTD cases negative biases of steady-state and weakening TCs improved little.

The improvement rate of the MAE stratified by types of Pmin change (Fig. 6a) showed that the performance of the Pmin forecasts for steady-state TCs improved by over 10% during the period FT = 24–48 h. The
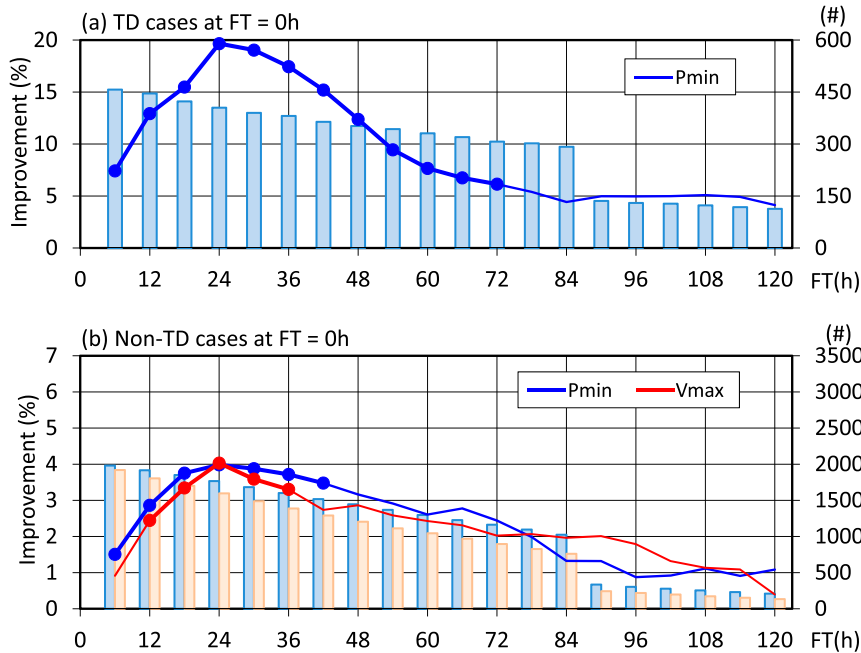
FIG. 4. (a) As in Fig. 3b, but for TD cases at FT = 0 h (Pmin only). (b) As in Fig. 3b, but for non-TD cases at FT = 0 h.

performance for intensifying TCs was slightly improved (2%–5%), whereas the performance for weakening TCs was not changed. As shown in Figs. 4 and 5, the suppression of overforecasting for weak initial TCs, including TDs, contributed to the substantial improvement of steady-state TCs. We describe the reason why the new predictors suppressed the overforecasting in the next subsection. For Vmax change (Fig. 6b), intensifying and steady-state TCs improved by a few percent. In contrast, the performance for weakening TCs was not changed.

To examine the improvement rate stratified by some conditions, MAEs of Pmin forecasts at FT = 48 h were plotted relative to the initial intensity (Fig. 7a), the actual intensity change (Fig. 7b), and the forecast intensity change (Fig. 7c). MAEs were decreased by the new predictors at initial intensities of 960 hPa and greater, where forecast samples accounted for 74% of the total. In particular, the improvement rate generally increased with increasing initial Pmin. This result is consistent with the great improvement for TD cases. MAEs relative to the actual intensity change indicated that improvement was seen at intensity changes between −20 and 10 hPa in 48 h, where the number of samples was greater than 80 in each bin (Fig. 7b). This result is related to the large improvement for steady-state TCs. For intensifying TCs whose Pmin fell between −55 and −85 hPa in 48 h, MAEs in SHIPS-GSMaP were decreased, although the number of samples was less than 50 in each bin and the

MAEs were still very large. MAEs relative to the forecast intensity change indicated that the peak of the samples was slightly displaced in the positive direction as a result of the suppression of overforecasting (Fig. 7c). In addition, the range of forecast intensity changes by SHIPS was narrower than the actual range shown in
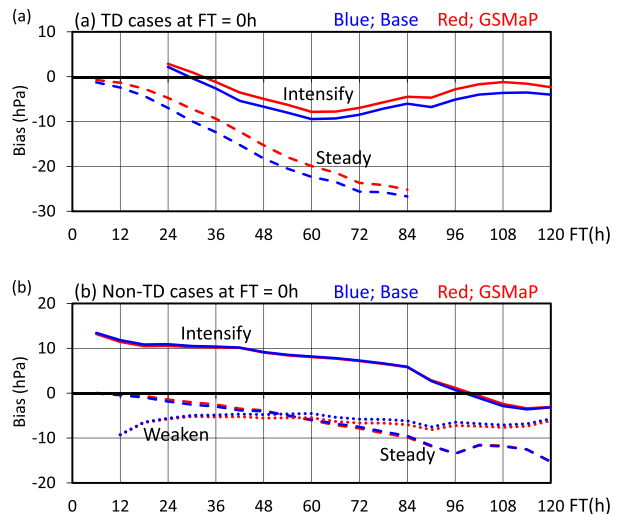

FIG. 5. Biases of the SHIPS-GSMaP and SHIPS-Base Pmin forecasts stratified by intensifying, weakening, and steady-state TCs. (a) TD cases at FT = 0 h. (b) Non-TD cases at FT = 0 h. Results with numbers of samples less than 50 are not shown.
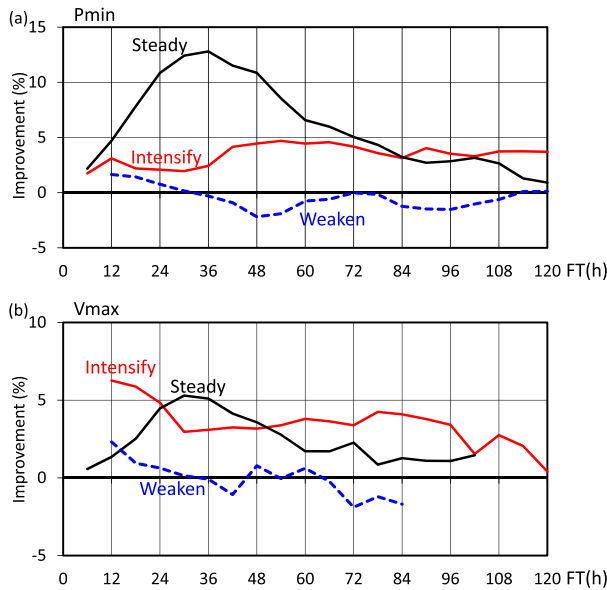
FIG. 6. Percent improvement of SHIPS-GSMaP MAEs relative to SHIPS-Base MAEs from 2013 to 2016 in the WNP basin stratified by intensifying, weakening, and steady-state TCs for (a) Pmin and (b) Vmax. Results with numbers of samples less than 50 are not shown.

Fig. 7b. The MAE increased when increasing the forecast intensity change.

We used AXIS and RVOL multiplied by OHC in this study. To examine the effect of the multiplication, we also tested SHIPS-GSMaP without the multiplication of OHC. The improvement was 1%–3% over SHIPS-Base, with little difference in the improvement between the Pmin and Vmax forecasts, and there was no peaked improvement for Pmin forecasts in the first half of the forecast period (Fig. 8a). By the multiplication of OHC, AXIS coefficients became greater (Figs. 8b,c), which greatly contributed to the decrease in negative biases of Pmin forecasts for TD cases (Fig. 5a) and contributed to the increase in the maximum improvement rate from 8% (not shown) to 20% (Fig. 4a) for TD cases. Weak TDs tend not to intensify shortly after their generation even when located over a high-OHC region. Forecast accuracy for such cases was greatly improved by the use of AXIS multiplied by OHC. In the next subsection, we present an example of the improvement.

b. Case study

As an example of the substantial improvement of TD cases, Fig. 9a shows a forecast result of a TD initialized at 1200 UTC 29 September 2013. This TD upgraded to TS Fitow (2013) in 30 h and reached typhoon strength in 120 h, at 1200 UTC 4 October 2013. Figure 9b shows
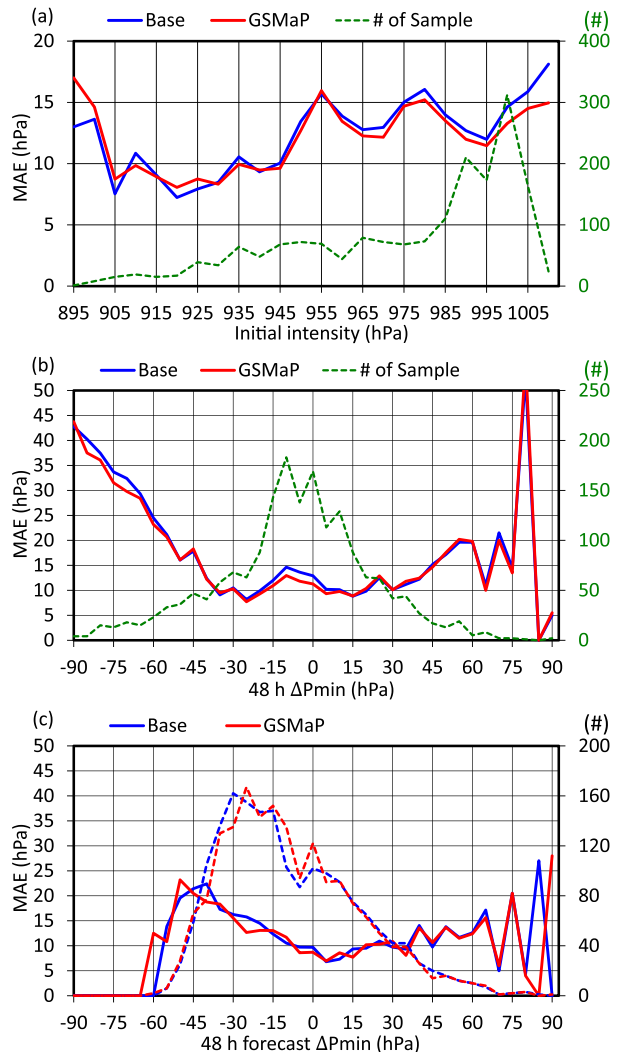

FIG. 7. SHIPS-Base and SHIPS-GSMaP MAEs for 48-h intensity forecasts in 5-hPa bins stratified by (a) best track initial intensity, (b) actual 48-h intensity change, and (c) forecast 48-h intensity change. Dashed lines represent the number of samples within a particular bin, corresponding to the y axis on the right.

contributions from OHC (a predictor named COHC) in SHIPS-Base, as well as COHC and AXIS in SHIPS-GSMaP, during the period FT = 6–72 h. In this forecast, contributions from the new predictors except AXIS, and differences in contributions from all other predictors between SHIPS-Base and SHIPS-GSMaP, were less than 4 hPa. The axisymmetry was very small, 29, at FT = 0 h, while OHC was greater than 140 kJ cm^{-2} up to FT = 54 h. SHIPS-Base forecast intensification because of the very high OHC. In contrast, in SHIPS-GSMaP, the contribution from COHC was greatly decreased and the contribution from AXIS was relatively small. As a result,
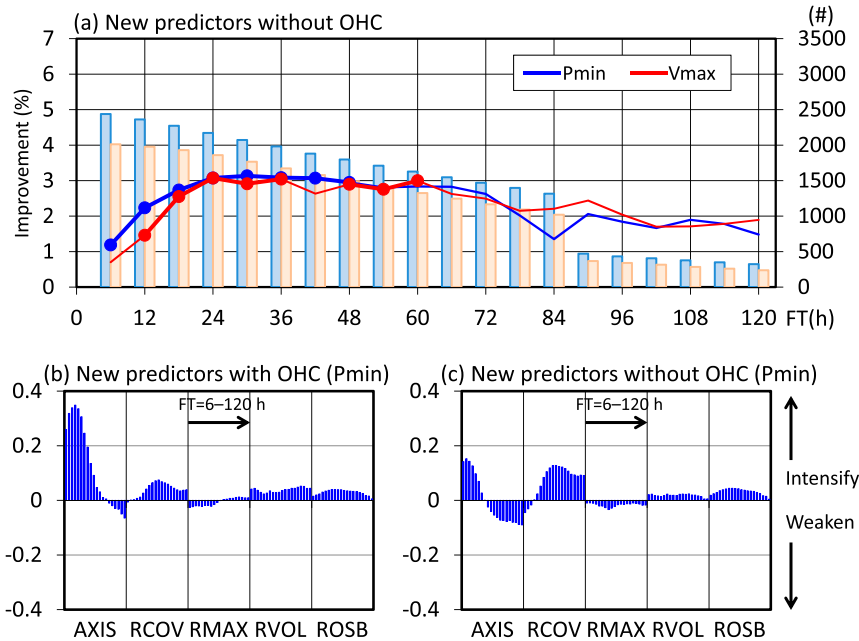
FIG. 8. (a) As in Fig. 3b, but for the new predictors without the multiplication of OHC. (b) As in Fig. 2a, but for only the new predictors with the multiplication of OHC. (c) As in Fig. 2a, but for only the new predictors without the multiplication of OHC.

SHIPS-GSMaP could improve, to some extent, the overforecasting of the TD. A statistical verification for all TD cases also confirmed the same trend (not shown), resulting in the suppression of overforecasting of TD cases (Fig. 5a).

The above result can be interpreted as follows. Statistically, within the linear regression framework, the intensification rate is proportional to OHC. In reality, however, TDs do not necessarily start intensifying shortly after their genesis, in particular when they have no organized convection around the storm center, no matter how high OHC is. As a result, SHIPS forecasts for TD cases tend to have negative biases (i.e., overforecasting) (Fig. 5a). This trend may be partly due to the fact that the training samples used did not include sufficient TD cases (Fig. 1a). Nonetheless, the multiplication of the axisymmetry by OHC can reasonably contribute to an intensity change: AXIS does not contribute to intensification when OHC is high but the axisymmetry is small, like the case of Typhoon Fitow (2013), and AXIS contributes to intensification when both OHC and the axisymmetry are high. Therefore, we found that the construction of nonlinear predictors using environmental conditions and inner-core features is important to effectively incorporate rainfall and structural information into the framework of a multiple linear regression.

Besides TD cases, the addition of the new predictors contributed to the suppression of overforecasting of monsoon-gyre-type TCs. Typhoon Nakri (2014) was a typical monsoon-gyre-type TC, which tends not to intensify greatly (Fig. 10). The intensity at 0000 UTC
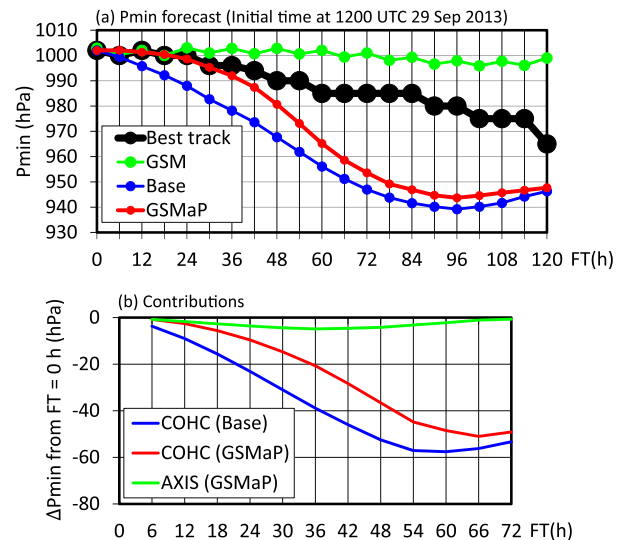

FIG. 9. (a) Intensity forecasts of the JMA GSM, SHIPS-Base, and SHIPS-GSMaP for a TD initialized at 1200 UTC 29 Sep 2013. Best track intensity is also plotted. (b) Contributions of SHIPS predictors (COHC and AXIS) to intensity changes shown in (a) during the period of FT = 6–72 h.
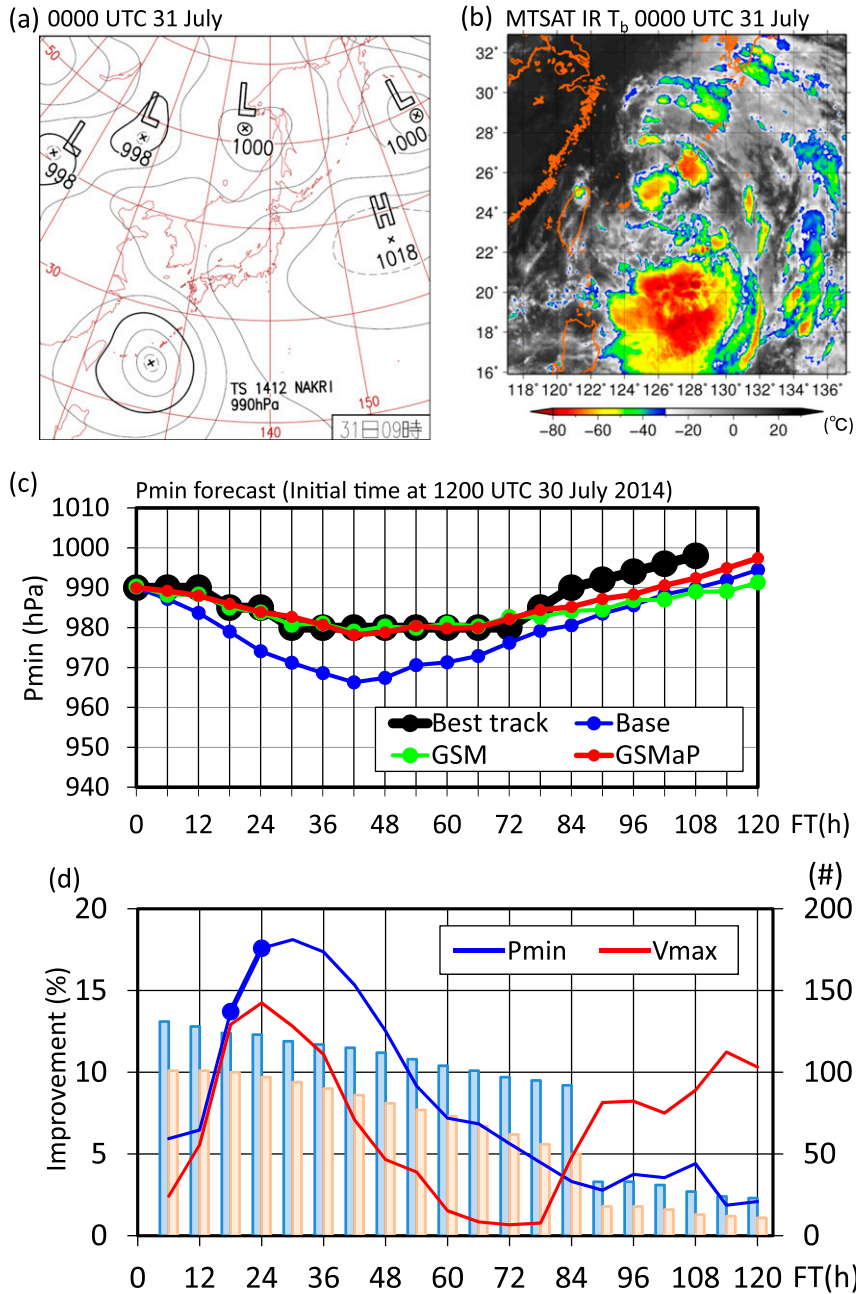
(a) 0000 UTC 31 July

(b) MTSAT IR T_b 0000 UTC 31 July

(c) Pmin forecast (Initial time at 1200 UTC 30 July 2014)

(d)

FIG. 10. (a) Weather chart at 0000 UTC 31 Jul 2014 provided by JMA. (b) Infrared brightness temperatures (at 10.3–11.3 μm) from the *Multifunctional Transport Satellite-2* (*MTSAT-2*) geostationary satellite at 0000 UTC 31 Jul 2014. (c) As in Fig. 9a, but for Typhoon Nakri (2014) initialized at 1200 UTC 30 Jul. Because Nakri weakened to a TD at FT = 90 h (0600 UTC 3 Aug 2014) and dissipated at FT = 114 h (0600 UTC 4 Aug 2014), there was no best track intensity after FT = 108 h. (d) As in Fig. 3b, but for TCs with longest R_{30} > 450 km just when they reach TS strength, including Typhoons Leepi (2013), Man-yi (2013), Pabuk (2013), Nakri (2014), Choi-wan (2015), and Omais (2016).

31 July 2014 (0900 Japan standard time) was a Pmin of 990 hPa (Fig. 10a) and had a 10-min Vmax of 40 kt, with a 30-kt radius of 700 km to the southeast and 500 km to the northwest. Although the size was relatively large,

no organized convection occurred around the center (24.4°N, 127.1°E) (Fig. 10b), and Pmin fell by only 10 hPa after 0000 UTC 31 July (Fig. 10c). SHIPS-Base initialized at 1200 UTC 30 July, however, forecast

intensification up to 967 hPa, because SSTs around the TC were greater than 29°C, and the vertical wind shear (SHDC) along the track was ~5 m s^{-1}. In contrast, the forecast of SHIPS-GSMaP was very good. All newly added predictors contributed to the suppression of the decrease in Pmin in the first half of the forecast period (not shown). We also selected similar TCs to Typhoon Nakri (2014) by using a simple definition of the largest $R_{30} > 450$ km just when the TCs reach TS strength. A statistical verification of forecasts for those TCs showed a marked improvement in SHIPS-GSMaP (Fig. 10d), although the number of samples was too small to have statistical significance.

In contrast, as shown in Fig. 6, SHIPS-GSMaP yielded slightly improved forecast skill for intensifying TCs. In the case of Typhoon Noul (2015) (Fig. 11a), which started to intensify at FT = 6 h, then weakened after FT = 24 h, there was little difference in the forecasts between SHIPS-GSMaP and SHIPS-Base during the intensification period. This result may be attributed to the slight correlation between the intensity change in the next 12–48 h and axisymmetry at current intensities < 960 hPa (see Fig. 7 in Shimada et al. 2017). In fact, compared to SHIPS-Base, AXIS contributed to the decrease in Pmin in SHIPS-GSMaP, but was offset by an enhanced increase in Pmin from the MSLP predictor (i.e., Pmin at FT = 0 h) and a weakened decrease in Pmin from the COHC predictor (Fig. 11b). This result is consistent with the fact that MAEs were not decreased by the new predictors at initial intensities < 960 hPa (Fig. 7a).

c. Real-time forecasts

The results of real-time forecasts showed that the improvement rate of Pmin forecasts in real-time SHIPS-GSMaP was slightly decreased, compared to SHIPS-GSMaP (Fig. 12). The improvement for Pmin during the period FT = 6–48 h was statistically significant at the 95% confidence level. The Vmax forecast was slightly improved during the period FT = 12–90 h, though the improvement was not statistically significant at the 95% confidence level. These results indicate the feasibility of SHIPS-GSMaP for operational use in real time.

The fact that SHIPS with the use of the GSMaP reanalysis product was superior to that with the use of the near-real-time GSMaP product suggests that more accurate rainfall and structural information can lead to a better intensity forecast and that the increase in the number of microwave satellites will lead to further improvement in real-time SHIPS-GSMaP. In this sense, the Time-Resolved Observations of Precipitation Structure and Storm Intensity with a Constellation of Smallsats (TROPICS) mission (Blackwell et al. 2018) will observe the precipitation distribution at high temporal
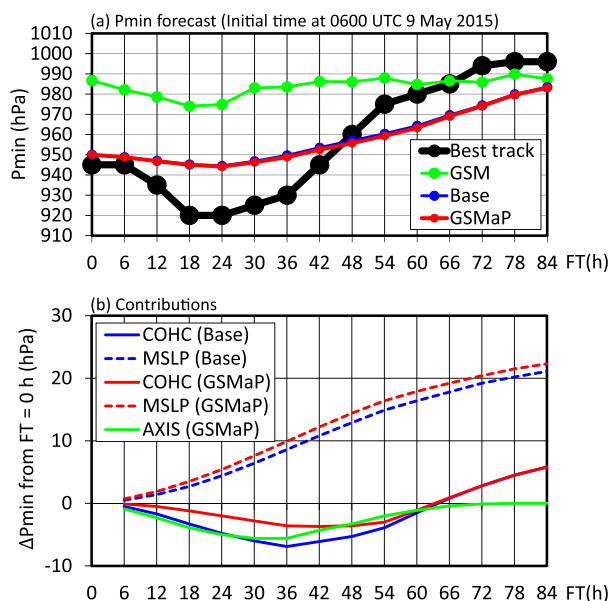

FIG. 11. (a) As in Fig. 9a, but for Typhoon Noul (2015) initialized at 0600 UTC 9 May 2015. Noul underwent extratropical transition at FT = 72 h (0600 UTC 12 May 2015). (b) Contributions of SHIPS predictors (COHC, MSLP, and AXIS) to intensity changes shown in (a).

resolution (~40 min on average) and would be expected to further improve the accuracy of real-time SHIPS-GSMaP in the future, if such data can be made available in near–real time.

4. Discussion

Hakim (2013) and Brown and Hakim (2013) demonstrated, using long-term simulated TC data in a situation free of the effects of environmental variability, that the intrinsic predictability time scale for mature, steadystate TCs was 2–3 days. Their findings are consistent with our results showing that the improvement within ~3 days was statistically significant at the 95% level. The fact that a few percent of improvement was retained after FT = 3 days in this study might be related to the differences in the forecast samples: the samples used in this study include a lot of weak initial TCs (Fig. 7a) that intensified afterward, whereas the samples used by Hakim (2013) and Brown and Hakim (2013) consist of mature, steady-state TCs.

The greatest improvement was obtained during a period of FT = 24–36 h, not a period of FT = 6–18 h. One possible reason for this is the impact of initial intensity errors on the improvement in SHIPS. As shown in Fig. 3a, an MAE of ~2.5 hPa or 2.5 kt existed at FT = 0 h in our experiment. This error can lead to errors in some of the predictors (e.g., PER, MSLP, OSLP, POT,
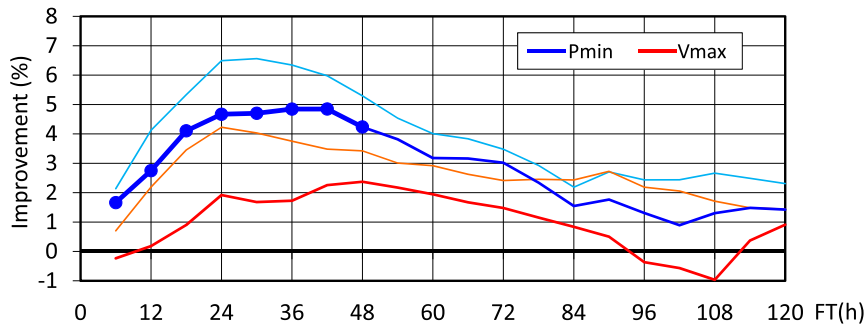
FIG. 12. Percent improvement in real-time SHIPS-GSMaP MAEs relative to SHIPS-Base MAEs from 2013 to 2016 in the WNP basin (blue line, Pmin; red line, Vmax). Bold lines with filled circles indicate statistically significant differences at the 95% level. For reference, the percent improvement of SHIPS-GSMaP MAEs shown in Fig. 3b is also indicated by the thin light blue (Pmin) and brown (Vmax) lines.

and POT2), which have large coefficients within FT = 24 h (Fig. 2). Thus, without improvement in the initial intensity errors, it is likely to be difficult to realize a large improvement during a period of FT = 6–18 h. This speculation is consistent with the suggestion by Emanuel and Zhang (2016), who demonstrated, using a simple coupled ocean–atmosphere model, that errors in initial intensity can dominantly affect the accuracy of intensity forecasts over the first 2–4 days.

Xu and Wang (2018) showed that an initial vortex with larger RMW and higher inertial stability outside the RMW takes longer to humidify the inner-core region for initial spinup due to the larger volume inside the RMW and weaker upward motion in the boundary layer. Emanuel and Zhang (2017) demonstrated that uncertainty in initial inner-core moisture information can dominantly affect the predictability of intensity forecasts up to several days ahead. These studies are consistent with the findings of this study that the addition of rainfall and structural features could further improve the accuracy of SHIPS that primarily uses environmental conditions.

Although improvement was obtained, the coefficients of the new predictors were relatively small, except for AXIS (Fig. 2), and the improvement for intensifying TCs was not high enough to improve the RI forecasts (e.g., Figs. 6 and 7b). Shimada et al. (2017) found a relationship between the axisymmetry and subsequent intensity change only during the intensification stage. Carrasco et al. (2014) also excluded weakening cases in their study. Cecil and Zipser (1999) showed that inner-core areal-mean 85-GHz T_b is highly correlated with future intensity (correlation coefficient ~0.7), but only slightly correlated with future intensity change (~0.25). These facts may explain the limited improvement in the linear regression framework between structural features and future intensity change.

5. Summary

The current version of SHIPS predicts TC intensity mainly using predictors associated with environmental conditions, without using rainfall and structural features of TCs. Recent studies, however, have pointed out that inner-core structural conditions, such as the axisymmetry of the rainfall distribution, also govern subsequent intensity change. We examined the degree to which the accuracy could be improved when rainfall and structural features of TCs were added to SHIPS for the WNP basin.

We derived new predictors mainly from the hourly GSMaP product, which is a microwave satellite-based rainfall estimate dataset. The predictors derived from the GSMaP product for the Pmin forecasts include the axisymmetry of rainfall structure within 300 km of the TC center, rain areal coverage within a radius of 100–300 km, the radius of maximum azimuthal mean rainfall, and the total volumetric rain within a radius of 100 km. Among these predictors, each value of the axisymmetry and the total volumetric rainfall was multiplied by OHC along a forecast track. In addition, the Rossby number, defined as the maximum wind divided by the product of the radius of 30-kt wind speed and the Coriolis parameter, was incorporated. Previous studies used predictors based on T_b data such as mean T_b and maximum T_b around the TC, whereas in this study we used predictors associated with physical features that were relevant to the intensity change found in previous studies. This modification facilitates the interpretation of the SHIPS forecasts.

SHIPS coefficients indicated that among the five new predictors, the axisymmetry multiplied by OHC (named AXIS) had the largest impact on the intensity change. First, we examined the degree to which the new predictors could improve the accuracy. In this examination,

the new predictors were derived from the GSMaP reanalysis product and best track data. The forecast results out to 5 days for TCs over the ocean showed that the addition of the new predictors for Pmin produced a 2%–7% improvement with a maximum improvement of just over 6% at FT = 24–36 h. The improvement for the Vmax forecast was over 3% during a period of FT = 18–54 h. For Pmin forecasts, substantial improvements (of up to 20%) were obtained for steady-state TCs and TD cases. AXIS contributed to the suppression of overforecasting of TD cases with low axisymmetry over high OHC regions. For both the Pmin and Vmax forecasts, the improvement rate was 1%–6% for intensifying TCs, while little improvement was found for weakening TCs.

We also performed a real-time forecast experiment, in which the new predictors were derived from the near-real-time hourly GSMaP product and real-time TC data. The results demonstrated that even the use of the near-real-time GSMaP product can improve the accuracy of SHIPS, confirming the feasibility of real-time SHIPS with the new predictors for operational use.

REFERENCES

Aberson, S. D., and M. DeMaria, 1994: Verification of a nested barotropic hurricane track forecast model (VICBAR). *Mon. Wea. Rev.*, **122**, 2804–2815, https://doi.org/10.1175/1520-0493(1994)122<2804:VOANBH>2.0.CO;2.

Alvey, G. R., III, J. Zawislak, and E. Zipser, 2015: Precipitation properties observed during tropical cyclone intensity change. *Mon. Wea. Rev.*, **143**, 4476–4492, https://doi.org/10.1175/MWR-D-15-0065.1.

Aonashi, K., and G. Liu, 2000: Passive microwave precipitation retrievals using TMI during the baiu period of 1998. Part I: Algorithm description and validation. *J. Appl. Meteor.*, **39**, 2024–2037, https://doi.org/10.1175/1520-0450(2000)039<2024:PMPRUT>2.0.CO;2.

——, and Coauthors, 2009: GSMaP passive microwave precipitation retrieval algorithm: Algorithm description and validation. *J. Meteor. Soc. Japan*, **87A**, 119–136, https://doi.org/10.2151/jmsj.87A.119.

Bankert, R. L., and P. M. Tag, 2002: An automated method to estimate tropical cyclone intensity using SSM/I imagery. *J. Appl. Meteor.*, **41**, 461–472, https://doi.org/10.1175/1520-0450(2002)041<0461:AAMTET>2.0.CO;2.

Blackwell, W. J., and Coauthors, 2018: An overview of the TROPICS NASA Earth Venture Mission. *Quart. J. Roy. Meteor. Soc.*, https://doi.org/10.1002/qj.3290, in press.

Brown, B. R., and G. J. Hakim, 2013: Variability and predictability of a three-dimensional hurricane in statistical equilibrium. *J. Atmos. Sci.*, **70**, 1806–1820, https://doi.org/10.1175/JAS-D-12-0112.1.

Cangialosi, J. P., and J. L. Franklin, 2017: 2016 hurricane season. National Hurricane Center Forecast Verification Rep., 72 pp., www.nhc.noaa.gov/verification/pdfs/Verification_2016.pdf.

Carrasco, C., C. Landsea, and Y. Lin, 2014: The influence of tropical cyclone size on its intensification. *Wea. Forecasting*, **29**, 582–590, https://doi.org/10.1175/WAF-D-13-00092.1.

Cecil, D. J., and E. J. Zipser, 1999: Relationships between tropical cyclone intensity and satellite-based indicators of inner core convection: 85-Ghz ice-scattering and lightning. *Mon. Wea. Rev.*, **127**, 103–123, https://doi.org/10.1175/1520-0493(1999)127<0103:RBTCIA>2.0.CO;2.

Chen, D. Y.-C., K. K. W. Cheung, and C.-S. Lee, 2011: Some implications of core regime wind structures in western North Pacific tropical cyclones. *Wea. Forecasting*, **26**, 61–75, https://doi.org/10.1175/2010WAF2222420.1.

DeMaria, M., 2010: Tropical cyclone intensity change predictability estimates using a statistical-dynamical model. *29th Conf. on Hurricanes and Tropical Meteorology*, Tucson, AZ, Amer. Meteor. Soc., 9C.5, https://ams.confex.com/ams/29Hurricanes/techprogram/paper_167916.htm.

——, and J. Kaplan, 1994: A statistical hurricane intensity prediction scheme (SHIPS) for the Atlantic basin. *Wea. Forecasting*, **9**, 209–220, https://doi.org/10.1175/1520-0434(1994)009<0209:ASHIPS>2.0.CO;2.

——, and ——, 1999: An updated Statistical Hurricane Intensity Prediction Scheme (SHIPS) for the Atlantic and eastern North Pacific basins. *Wea. Forecasting*, **14**, 326–337, https://doi.org/10.1175/1520-0434(1999)014<0326:AUSHIP>2.0.CO;2.

——, M. Mainelli, L. K. Shay, J. A. Knaff, and J. Kaplan, 2005: Further improvements to the Statistical Hurricane Intensity Prediction Scheme (SHIPS). *Wea. Forecasting*, **20**, 531–543, https://doi.org/10.1175/WAF862.1.

——, C. R. Sampson, J. A. Knaff, and K. D. Musgrave, 2014: Is tropical cyclone intensity guidance improving? *Bull. Amer. Meteor. Soc.*, **95**, 387–398, https://doi.org/10.1175/BAMS-D-12-00240.1.

Emanuel, K., and F. Zhang, 2016: On the predictability and error sources of tropical cyclone intensity forecasts. *J. Atmos. Sci.*, **73**, 3739–3747, https://doi.org/10.1175/JAS-D-16-0100.1.

——, and ——, 2017: The role of inner-core moisture in tropical cyclone predictability and practical forecast skill. *J. Atmos. Sci.*, **74**, 2315–2324, https://doi.org/10.1175/JAS-D-17-0008.1.

Hakim, G. J., 2013: The variability and predictability of axisymmetric hurricanes in statistical equilibrium. *J. Atmos. Sci.*, **70**, 993–1005, https://doi.org/10.1175/JAS-D-12-0188.1.

Hendricks, E. A., M. S. Peng, B. Fu, and T. Li, 2010: Quantifying environmental control on tropical cyclone intensity change. *Mon. Wea. Rev.*, **138**, 3243–3271, https://doi.org/10.1175/2010MWR3185.1.

Hoshino, S., and T. Nakazawa, 2007: Estimation of tropical cyclone's intensity using TRMM/TMI brightness temperature data. *J. Meteor. Soc. Japan*, **85**, 437–454, https://doi.org/10.2151/jmsj.85.437.

Ishii, M., A. Shouji, S. Sugimoto, and T. Matsumoto, 2005: Objective analyses of sea-surface temperature and marine meteorological variables for the 20th century using ICOADS and the Kobe Collection. *Int. J. Climatol.*, **25**, 865–879, https://doi.org/10.1002/joc.1169.

Jarvinen, B. R., and C. J. Neumann, 1979: Statistical forecasts of tropical cyclone intensity for the North Atlantic basin. NOAA

Tech. Memo. NWS NHC-10, 22 pp., http://www.nhc.noaa.gov/pdf/NWS-NHC-1979-10.pdf.

JAXA, 2018a: JAXA global rainfall watch. Japan Aerospace Exploration Agency, accessed 8 February 2018, http://sharaku.eorc.jaxa.jp/GSMaP/index.htm.

——, 2018b: JAXA realtime rainfall watch. Japan Aerospace Exploration Agency, accessed 8 February 2018, http://sharaku.eorc.jaxa.jp/GSMaP_NOW/index.htm.

Jiang, H., and E. M. Ramirez, 2013: Necessary conditions for tropical cyclone rapid intensification as derived from 11 years of TRMM data. *J. Climate*, **26**, 6459–6470, https://doi.org/10.1175/JCLI-D-12-00432.1.

JMA, 2018: JMA numerical weather prediction. Japan Meteorological Agency, http://www.jma.go.jp/jma/jma-eng/jma-center/nwp/nwp-top.htm.

Jones, T. A., and D. J. Cecil, 2007: SHIPS-MI forecast analysis of Hurricanes Claudette (2003), Isabel (2003), and Dora (1999). *Wea. Forecasting*, **22**, 689–707, https://doi.org/10.1175/WAF1016.1.

——, ——, and M. DeMaria, 2006: Passive-microwave-enhanced Statistical Hurricane Intensity Prediction Scheme. *Wea. Forecasting*, **21**, 613–635, https://doi.org/10.1175/WAF941.1.

——, ——, and J. Dunion, 2007: The environmental and inner-core conditions governing the intensity of Hurricane Erin (2007). *Wea. Forecasting*, **22**, 708–725, https://doi.org/10.1175/WAF1017.1.

Kieper, M., and H. Jiang, 2012: Predicting tropical cyclone rapid intensification using the 37 GHz ring pattern identified from passive microwave measurements. *Geophys. Res. Lett.*, **39**, L13804, https://doi.org/10.1029/2012GL052115.

Knaff, J. A., M. DeMaria, B. Sampson, and J. M. Gross, 2003: Statistical, 5-day tropical cyclone intensity forecasts derived from climatology and persistence. *Wea. Forecasting*, **18**, 80–92, https://doi.org/10.1175/1520-0434(2003)018<0080:SDTCIF>2.0.CO;2.

——, C. R. Sampson, and M. DeMaria, 2005: An operational statistical typhoon intensity prediction scheme for the western North Pacific. *Wea. Forecasting*, **20**, 688–699, https://doi.org/10.1175/WAF863.1.

Kobayashi, S., and Coauthors, 2015: The JRA-55 reanalysis: General specifications and basic characteristics. *J. Meteor. Soc. Japan*, **93**, 5–48, https://doi.org/10.2151/jmsj.2015-001.

Kubota, T., and Coauthors, 2007: Global precipitation map using satellite-borne microwave radiometers by the GSMaP project: Production and validation. *IEEE Trans. Geosci. Remote Sens.*, **45**, 2259–2275, https://doi.org/10.1109/TGRS.2007.895337.

——, S. Shige, K. Aonashi, and K. Okamoto, 2009: Development of nonuniform beamfilling correction method in rainfall retrievals for passive microwave radiometers over ocean using TRMM observations. *J. Meteor. Soc. Japan*, **87A**, 153–164, https://doi.org/10.2151/jmsj.87A.153.

Kurihara, Y., T. Sakurai, and T. Kuragano, 2006: Global daily sea surface temperature analysis using data from satellite microwave radiometer, satellite infrared radiometer and in-situ observations (in Japanese). *Wea. Bull.*, **73**, S1–S18.

Lander, M. A., 1994: Description of a monsoon gyre and its effects on the tropical cyclones in the western North Pacific during August 1991. *Wea. Forecasting*, **9**, 640–654, https://doi.org/10.1175/1520-0434(1994)009<0640:DOAMGA>2.0.CO;2.

——, 1996: Specific tropical cyclone track types and unusual tropical cyclone motions associated with a reverse-oriented monsoon trough in the western North Pacific. *Wea. Forecasting*, **11**, 170–186, https://doi.org/10.1175/1520-0434(1996)011<0170:STCTTA>2.0.CO;2.

Miyamoto, Y., and T. Takemi, 2013: A transition mechanism for the axisymmetric spontaneous intensification of tropical cyclones. *J. Atmos. Sci.*, **70**, 112–129, https://doi.org/10.1175/JAS-D-11-0285.1.

——, and ——, 2015: A triggering mechanism for rapid intensification of tropical cyclones. *J. Atmos. Sci.*, **72**, 2666–2681, https://doi.org/10.1175/JAS-D-14-0193.1.

Rao, G. V., and P. D. MacArthur, 1994: The SSM/I estimated rainfall amounts of tropical cyclones and their potential in predicting the cyclone intensity changes. *Mon. Wea. Rev.*, **122**, 1568–1574, https://doi.org/10.1175/1520-0493(1994)122<1568:TSERAO>2.0.CO;2.

——, and J. H. McCoy, 1997: SSM/I measured microwave brightness temperatures (TB's), anomalies of TB's, and their relationship to typhoon intensification. *Nat. Hazards*, **15**, 1–19, https://doi.org/10.1023/A:1007963829299.

Rappaport, E. N., J.-G. Jiing, C. W. Landsea, S. T. Murillo, and J. L. Franklin, 2012: The Joint Hurricane Test Bed: Its first decade of tropical cyclone research-to-operations activities reviewed. *Bull. Amer. Meteor. Soc.*, **93**, 371–380, https://doi.org/10.1175/BAMS-D-11-00037.1.

Sampson, C. R., and J. A. Knaff, 2014: Advances in intensity guidance. *Eighth Int. Workshop on Tropical Cyclones*, Jeju, South Korea, WMO, https://www.wmo.int/pages/prog/arep/wwrp/new/documents/Topic2.7_AdvancesinIntensityGuidance.pdf.

Schumacher, A., M. DeMaria, and J. Knaff, 2013: Summary of the new statistical-dynamical intensity forecast models for the Indian Ocean and Southern Hemisphere and resulting performance. JTWC Project Final Rep., 11 pp., http://rammb.cira.colostate.edu/research/tropical_cyclones/ships/docs/JTWC_project_final_report_oct_2013.docx.

Shige, S., and Coauthors, 2009: The GSMaP precipitation retrieval algorithm for microwave sounders. Part I: Over-ocean algorithm. *IEEE Trans. Geosci. Remote Sens.*, **47**, 3084–3097, https://doi.org/10.1109/TGRS.2009.2019954.

Shimada, U., K. Aonashi, and Y. Miyamoto, 2017: Tropical cyclone intensity change and axisymmetricity deduced from GSMaP. *Mon. Wea. Rev.*, **145**, 1003–1017, https://doi.org/10.1175/MWR-D-16-0244.1.

Ushio, T., and Coauthors, 2009: A Kalman filter approach to the Global Satellite Mapping of Precipitation (GSMaP) from combined passive microwave and infrared radiometric data. *J. Meteor. Soc. Japan*, **87A**, 137–151, https://doi.org/10.2151/jmsj.87A.137.

Usui, N., S. Ishizaki, Y. Fujii, H. Tsujino, T. Yasuda, and M. Kamachi, 2006: Meteorological Research Institute multivariate ocean variational estimation (MOVE) system: Some early results. *Adv. Space Res.*, **37**, 806–822, https://doi.org/10.1016/j.asr.2005.09.022.

Wilks, D. S., 2006: *Statistical Methods in the Atmospheric Sciences*. 2nd ed. Academic Press, 627 pp.

Xu, J., and Y. Wang, 2018: Effect of the initial vortex structure on intensification of a numerically simulated tropical cyclone. *J. Meteor. Soc. Japan*, **96**, 111–126, https://doi.org/10.2151/jmsj.2018-014.

Yamaguchi, M., J. Ishida, H. Sato, and M. Nakagawa, 2017: WGNE intercomparison of tropical cyclone forecasts by operational NWP models: A quarter-century and beyond. *Bull. Amer. Meteor. Soc.*, **98**, 2337–2349, https://doi.org/10.1175/BAMS-D-16-0133.1.

——, H. Owada, U. Shimada, M. Sawada, T. Iriguchi, K. D. Musgrave, and M. DeMaria, 2018: Tropical cyclone intensity prediction in the western North Pacific basin using SHIPS and JMA/GSM. *SOLA*, **14**, 138–143, https://doi.org/10.2151/sola.2018-024.

Zagrodnik, J. P., and H. Jiang, 2014: Rainfall, convection, and latent heating distributions in rapidly intensifying tropical cyclones. *J. Atmos. Sci.*, **71**, 2789–2809, https://doi.org/10.1175/JAS-D-13-0314.1.